Journal of Biomedical Optics

BiomedicalOptics.SPIEDigitalLibrary.org

Computational model of bladder tissue based on its measured optical properties

Ilya E. Rafailov
Victor V. Dremin
Karina S. Litvinova
Andrey V. Dunaev
Sergei G. Sokolovski
Edik U. Rafailov

SPIE.

Computational model of bladder tissue based on its measured optical properties

Ilya E. Rafailov,[a,*] Victor V. Dremin,[b] Karina S. Litvinova,[c] Andrey V. Dunaev,[b] Sergei G. Sokolovski,[c] and Edik U. Rafailov[c]

[a]Aston University, School of Engineering and Applied Sciences, Aston Institute of Photonic Technologies, Birmingham B4 7ET, United Kingdom
[b]State University—Education-Science-Production Complex, Biomedical Photonics Instrumentation Group, Scientific-Educational Centre of "Biomedical Engineering," Oryol 302020, Russia
[c]Aston University, Optoelectronics and Biomedical Photonics Group, Aston Institute of Photonic Technologies, Aston Triangle, Birmingham B4 7ET, United Kingdom

Abstract. Urinary bladder diseases are a common problem throughout the world and often difficult to accurately diagnose. Furthermore, they pose a heavy financial burden on health services. Urinary bladder tissue from male pigs was spectrophotometrically measured and the resulting data used to calculate the absorption, transmission, and reflectance parameters, along with the derived coefficients of scattering and absorption. These were employed to create a "generic" computational bladder model based on optical properties, simulating the propagation of photons through the tissue at different wavelengths. Using the Monte-Carlo method and fluorescence spectra of UV and blue excited wavelength, diagnostically important biomarkers were modeled. Additionally, the multifunctional noninvasive diagnostics system "LAKK-M" was used to gather fluorescence data to further provide essential comparisons. The ultimate goal of the study was to successfully simulate the effects of varying excited radiation wavelengths on bladder tissue to determine the effectiveness of photonics diagnostic devices. With increased accuracy, this model could be used to reliably aid in differentiating healthy and pathological tissues within the bladder and potentially other hollow organs. [DOI: 10.1117/1.JBO.21.2.025006]

Keywords: urinary bladder cancer; Monte-Carlo; three-dimensional model; fluorescence spectroscopy; optical properties; tissue.

Paper 150699PRR received Oct. 20, 2015; accepted for publication Jan. 14, 2016; published online Feb. 15, 2016.

1 Introduction

Photonics-based techniques have, for years, been some of the most effective methods of screening, diagnosis, and treatment in many medical conditions.[1,2] This role has presented itself to be particularly vital for research into numerous forms of cancer. Urinary bladder cancer (BC) is of special interest, due to its position as one of the top 10 most prevalent and expensive cancers in the world.[3,4] Cases of aggressive muscle invasive and metastatic disease exhibit high fatality figures. Even non-muscle-invasive disease (accounting for around 70% of cases), which is generally nonfatal, experiences high rates of recurrence and progression, resulting in considerable patient morbidity.[5]

The high rates of recurrence and progression associated with BC make it the single most expensive cancer to treat on a per-patient basis.[3,4] It is also important to note that bladder tumors are classified as muscle invasive and noninvasive. The noninvasive tumors consist of carcinoma *in situ* (CIS) appearing as flat tumors present on the mucosa surface, pTa papillary tumors that reside in the mucosa, and the pT1 tumors that have penetrated the lamina propria, but not the muscle tissue layers. Stages pT2 to pT4 describe muscle-invasive tumors based on the extent of the tumor penetration into the tissue layers. These tumors are considered highly malignant and are known to metastasize into other regions such as the lungs.[6] The early detection of BC is, therefore, imperative. In contrast to deeper lying organs, such as the liver and kidneys, use of endoscopes provides easy transurethral access to the bladder, avoiding complex surgery or laparoscopy. As such, it lends itself well to photonics diagnostics using cystoscopic probes and has been the focus of numerous advances in minimally invasive diagnosis research over the years.[7] Despite this, urine cytology, transurethral resection of the bladder tumor (TURBT), white light cystoscopy (WLC), and photodynamic diagnosis (PDD) are still considered the gold standards for both diagnosis and treatment.[8] However, TURBT is an invasive procedure and both WLC and PDD suffer from their own respective limitations.[9,10] Presence of inflamed or infected mucosa can further exacerbate these drawbacks.[8] Additionally, neither technique provides direct evidence of changes and interaction at a molecular level, only being capable of providing a visual representation of the surface of the tissue.

Recent advances in biophotonics (improved cost effectiveness of techniques, signal-to-noise ratio, and tissue penetration depth by laser irradiation) have provided potential new avenues for diagnosis of BC through detection and quantification of endogenous tissue fluorescence without the need for fluorescent dyes.[11–13] Numerous endogenous molecules naturally fluoresce when excited with the appropriate wavelength of light. Analysis of tissue autofluorescence spectra under different excitation wavelengths can therefore provide valuable information on tissue architecture, metabolism activity, and disorders.[12–14] Such analysis has already produced a number of specific spectra for tumors of the skin, gastrointestinal tract, urogenital systems, and mouth mucous membranes.[15] So far, fluorescence spectroscopy

*Address all correspondence to: Ilya E. Rafailov, E-mail: rafailoi@aston.ac.uk

1083-3668/2016/$25.00

(FS) and autofluorescence have been shown to exhibit high specificity and sensitivity during the differential diagnosis of tissue dysplasia, adenoma, and adenocarcinoma.[15–17] Among the most diagnostically relevant biomarkers are the mitochondrial cofactors NADH and FAD, and the structural protein collagen. NADH and FAD provide information on metabolic changes undertaken by cancer cells, with the optical redox ratio (NADH/FAD) showing promise in the diagnosis and monitoring of several cancers, owing to selective accumulation of NADH in cancer cells.[15,16,18] Conversely, during tumor progression, collagen can often provide a diagnostic signal due to its reduction in the tissue.[19] It is proposed that this approach can act as a best of both worlds, providing high sensitivity for the diagnosis of early cancers without having to compromise on specificity. Autofluorescence spectroscopy has already proven itself a worthwhile diagnostic tool for the discrimination of many diseases[20–24] and has even exhibited differentiation between various types of benign and malignant tumors.[25] Further work is currently underway to reliably characterize the autofluorescence properties of healthy and malignant bladder tissue, both *ex vivo*[26] and *in vivo*.[7]

Autofluorescence spectroscopy depends crucially on understanding the interactions between light and tissue, with complex systems requiring analysis beyond simply measuring emitted fluorescence. Overlapping spectra of the fluorophores may be present in the resulting spectrum.[27] Furthermore, processes such as scattering and nonspecific absorption of both incident and emitted light often obscure the signals we obtain from tissue. These processes become significant obstacles the deeper we look into tissue and account for one of the main reasons why it is so difficult to detect early-grade bladder tumors and CIS. Needless to say, tissues with different optical properties result in variations of these processes, which must be taken into account when designing diagnostic techniques.[28] Furthermore, the multilayered nature of tissues like the bladder dramatically changes the passage and properties of light. Many previous studies in the field of autofluorescence spectroscopy have not taken into account the scattering and absorptive effects of different tissue layers. Many accounts have also suffered from falsely attributing malignancy-induced changes in tissue optical properties to absolute increases or decreases in tissue fluorophores. This is especially noticeable when matrix degradation or tissue thickening occurs.[29,30]

With autofluorescence becoming more widespread as a diagnostics technique, more effort has been made to reduce or circumvent its drawbacks. Tissue models, three-dimensional (3-D) and otherwise, are becoming commonplace to allow researchers to adequately model experiments, interpret results, and as initial tests for photonics-based equipment.[31–34] Certain groups have been involved in the development of 3-D bladder models, particularly physical optical phantoms.[35] Mainly constructed using optical coherence tomography data, they have already provided a wealth of information for the design and improvement of WLC and PDD. To this date, however, the authors know of no other groups working on reliable optical bladder models for the study of tissue autofluorescence, which take into account fluorescence contributions of distinct endogenous fluorophores. Minimally invasive diagnostic systems functionally capable of measuring autofluorescence spectra possess immense potential for the early detection of BC, but require a great deal of metrological support and rigorous characterization and testing before they can be employed in a clinical setting. Here, we have aimed to further develop our previously described computer simulated optical 3-D bladder model[36] to allow the study of light propagation of a wide range of wavelengths through bladder tissue. We determined the absorption and scattering parameters by measuring samples of pig bladder tissue and used FS over a range of wavelengths to measure tissue fluorescence for distinct fluorophores such as NADH, FAD, and collagen. We suggest the use of this model for directly comparing a host of photonic devices to determine their clinical worth. The effects of BC progression on the bladder tissue optical properties can also be modeled, providing diagnostic benchmarks by which to set tumor staging and grading criteria.

2 Methods

2.1 *Pig Bladder Analysis—Inverse Adding–Doubling Method*

Bladders from locally slaughtered male pigs ($n = 3$) were provided refrigerated and vacuum packed by an established supplier (WETLAB) and immediately refrigerated. Superior and lateral bladder surfaces (apical surface) were separated from the anteroinferior surface (basal surface) of the bladder using medical grade scalpel. Subsequently, 2 cm^2 sections (of 6- to 10-mm thickness) from each half were excised for analysis. Excised tissue was introduced into a specialized tissue clamp and fixed inside the spectrometer beam path for analysis. A Lambda 1050 spectrophotometer with a specialized integrating sphere module was used to record the absorption, transmission, and reflectance (diffuse) measurements. Samples were analyzed in the spectrophotometer for all three parameters in 1.5-nm increments across a wavelength range of 350 to 1800 nm. All spectrophotometric procedures were performed at room temperatures (22°C). Spectrophotometry data were visualized graphically using Origin Pro 8 software (Fig. 1). Laboratory facilities housing spectrometric devices used in this procedure were kept at steady room temperatures. To prevent drying and deterioration of tissue, samples were transported and maintained in small, covered petri dishes on a bed of dry ice at all times. These covers were kept on to reduce air exposure. Samples kept in the open for long periods of time between experiments were also sealed in their petri dishes with parafilm to further reduce exposure.

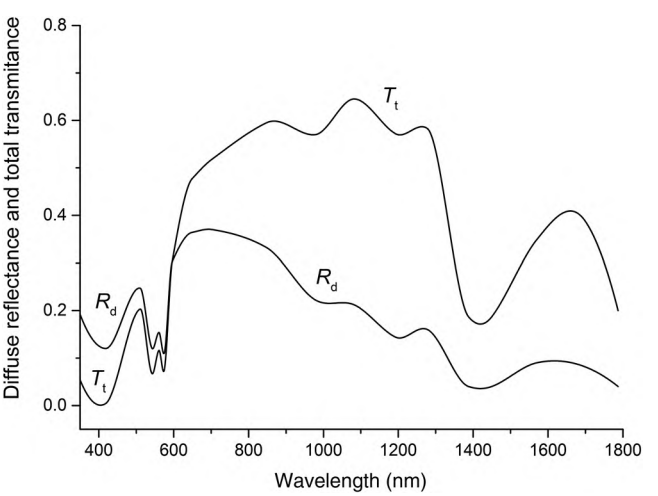

Fig. 1 Total transmittance (Tt) and diffuse reflectance (Rd) spectra obtained from 2-mm-thick pig urinary bladder.

To process the experimental results and determine the optical parameters, a combination of the inverse adding–doubling (IAD) method with a corrective Monte-Carlo calculation was used.[37,38] These methods are widely employed in tissue optics for processing data obtained by integrating sphere enabled spectrophotometry.

The IAD method allows for the determination of tissue absorption and scattering coefficients using the values of the diffuse reflectance and total transmission coefficients. The anisotropy factor (g) was fixed during the calculations. For the purpose of this paper, g was taken as 0.9 due to this value being most typical for the majority of biological tissues in the visible and near-infrared spectral wavelengths.[39]

The solutions to the series of Eqs. (1) and (2) were used as the initial values of μ_a and μ_s'

$$\frac{\mu_s'}{\mu_a+\mu_s'} = \begin{cases} 1-\left(\frac{1-4R_d-T_t}{1-T_t}\right)^2, & \text{if } \frac{R_d}{1-T_t} < 0.1 \\ 1-\frac{4}{9}\left(\frac{1-R_d-T_t}{1-T_t}\right)^2, & \text{if } \frac{R_d}{1-T_t} \geq 0.1 \end{cases}, \tag{1}$$

$$(\mu_a+\mu_s')l = \begin{cases} -\frac{\ln T_t \ln(0.05)}{\ln R_d}, & \text{if } R_d \leq 0.1 \\ 2^{1+5(R_d+T_t)}, & \text{if } R_d > 0.1 \end{cases}, \tag{2}$$

where R_d is the measured value for diffuse reflectance, T_t is the measured value for total transmission, and l is the thickness of the tissue.

The Monte-Carlo method was used to correct for the light loss at the sample edges, which is not collected by the integrating sphere. The calculated lost light for a given set of optical properties was taken into account within the subsequent iteration of the calculation using the adding–doubling method. This process was repeated as long as the optical properties were not stable, i.e., until the changes of calculated scattering and absorption values were less than 0.01 mm^{-1} between iterations.

2.2 *Construction of Three-Dimensional Model*

TracePro (Lambda Software) was used for the construction of the model. The creation of two layers (mucosa and muscle) and simulation of NADH and FAD was carried out following an identical procedure to that described in Rafailov et al.[36]

2.3 *Simulation of Fluorescence*

TracePro software was further used to simulate fluorescence from the above-constructed model. It employs fluorescent properties along with the material properties of the modeled tissue as well as the laws described previously in Rafailov et al.[36] The relative absorption $ab(\lambda)$ and relative excitation $ex(\lambda)$ are two major parameters that can be set and normalized to the molar extinction coefficient K_{peak} and the relative emission $em(\lambda)$. Input of the molar concentration C_{molar} is used to set the fluorescent material concentration. The fluorophore absorption coefficient in media is determined by

$$\mu_a(\lambda) = ab(\lambda)K_{peak}C_{molar}. \tag{3}$$

With the path length before absorption

$$d(\lambda) = -\log 10(x)/\mu_a(\lambda), \tag{4}$$

where x is a random value between 0 and 1.

Ascribing quantum efficiency to the system determines the number of photons involved in the simulation process.

2.4 *Fluorescence Measurement of Urinary Bladder Tissue*

Urinary bladder tissue was obtained as previously described and was split between dome and trigone sections. The bisected bladder was "virtually" divided into 16 sections. Virtual sections of the inner mucosal layer of the bladder were sequentially subjected to optical analysis by the fluorescence spectroscope of an "LAKK-M" multifunctional laser-based noninvasive diagnostic device. The fiber of the device was run along the length of its stand and the probe was placed into direct contact with the bladder tissue. No extra force was applied to the probe. Tissue was scanned sequentially using four different excitation sources (UV 365 nm, blue 450 nm, green 532 nm, and red 635 nm). Five seconds of contact was allocated per wavelength measurement. Resultant tissue fluorescence was recorded across a wavelength range of 300 to 800 nm using an inbuilt spectrometer and processed using custom-made software (LDF 3v3.1.1.403, SPE "LAZMA"). Data were exported and visualized graphically using Origin Pro 8 software. The entire procedure was carried out at room temperature, in a windowless dark room to limit noise.

3 Results

3.1 *Pig Bladder Analysis—Inverse Adding–Doubling Method*

For the construction of the 3-D model, the required transport coefficients of tissue were calculated from the experimentally obtained transmission and diffuse reflectance values. Thus, using IAD method-based modeling, absorption and scattering coefficient spectra were reconstructed [Figs. 2(a) and 2(b), respectively].

Experimental data presented in Ref. 40 are provided for comparison in Fig. 2. The result of calculated tissue penetration depth is displayed on Fig. 3. The evaluation of this depth in biological tissue was achieved using

$$\delta = \frac{1}{\sqrt{3\mu_a(\mu_a+\mu_s')}}. \tag{5}$$

3.2 *Three-Dimensional Model*

Due to the complex structural nature of organic tissue (in our case the urinary bladder), for the purposes of the theoretical modeling described in this paper, we constructed a simplified dual-layer model (mucosa and muscle).

Figure 4 displays the side and 3-D views of the constructed model simulating UV (a) and blue (b) light irradiation within the tissue. As it is evident from Fig. 3, the diagnostic depth into the tissue is around 1 to 1.2 mm.

3.3 *Measured and Modeled Fluorescence*

The results of experimental urinary bladder fluorescence at 365 and 450 nm excitation were compared to a simulated curve produced using the 3-D model (displayed in Fig. 5). This simulation incorporates NADH + collagen or FAD + collagen presence in the tissue.

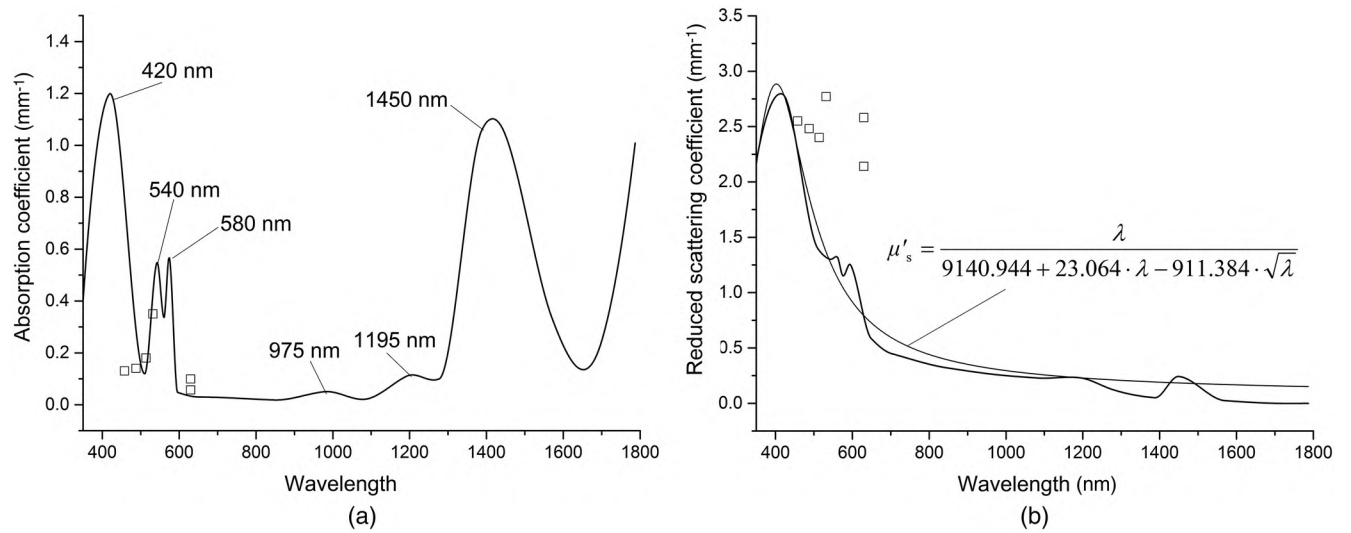

Fig. 2 (a) The absorption coefficient of pig urinary bladder and (b) the reduced scattering coefficient of pig urinary bladder. Experimental data from Staveren[40] are portrayed on the spectrum.

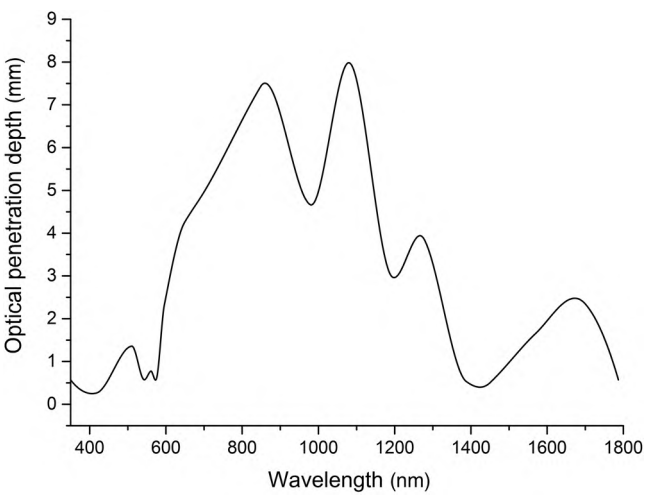

Fig. 3 The light penetration depth in urinary bladder tissue.

4 Discussion

4.1 *Pig Bladder Analysis—Inverse Adding–Doubling Method*

This study aimed to create a computer simulated optical 3-D bladder model for observing the propagation of light through bladder tissue. Looking at Fig. 2, the absorption bands of blood hemoglobin (420, 540, and 580 nm) and water (1450 nm) are clearly visible in the absorption spectra. The water peaks at 975 and 1195 nm, however, are less pronounced.

A drop in the scattering coefficient value is noticeable as wavelength increases, which is consistent with the general behavior of biological tissue scattering characteristics. The deviation from the monotony can be explained by the influence of strong absorption in the abovementioned areas.

As previously obtained data from the literature[40] are presented with our experimentally calculated transport coefficients, we are able to compare these outcomes. It is evident that they are in good agreement, with some of the observable differences attributed to the employment of different methods of experimental data processing, as well as differences in the properties of specific biological tissue samples.

It should be noted that the resulting dependence of the scattering coefficient, within the range of interest, could be approximated with high accuracy ($R^2 = 0.97$) using the Gunary power function[41]

$$\mu_s' = \frac{\lambda}{9140.944 + 23.064 \cdot \lambda - 911.384 \cdot \sqrt{\lambda}}. \quad (6)$$

Light penetration depth is one of the most critical characteristics for determining the capabilities of various methods of noninvasive optical diagnosis, including FS. Looking at Fig. 3, we can tell that this light penetration depth is around 0.5 to 2 mm in the spectral region of interest for fluorescent spectroscopy (350 to 600 nm). This allows for the stimulation of major biomarker (NADH, FAD, collagen, and so on) fluorescence.

Furthermore, use of experimentally obtained optical property data poses a distinct advantage over using literature-based data as displayed in our previous work.[36] Tissue samples spectroscopically measured for their reflectance and transmission properties were treated and kept at identical conditions to those undergoing fluorescence analyses, greatly reducing potential errors that arise from variation in laboratory conditions and different experimental practices. This also provides an avenue for further improvement of the calculated data by continuously expanding the sample size of experimentally measured tissue properties.

Following the calculation of transport coefficients, they were used in TracePro software (Lambda Research Corporation) to build the 3-D model.

4.2 *Three-Dimensional Model*

The construction of the 3-D model was based on the Monte Carlo methodology, which remains one of the most effective simulation tools when dealing with biological tissues. This is especially true for multilayered tissues. Thus, a number of other studies have applied this methodology to create models based on tissue optical properties.[42–45] These incorporate multiple layers ranging from a single[44] to five[46] different

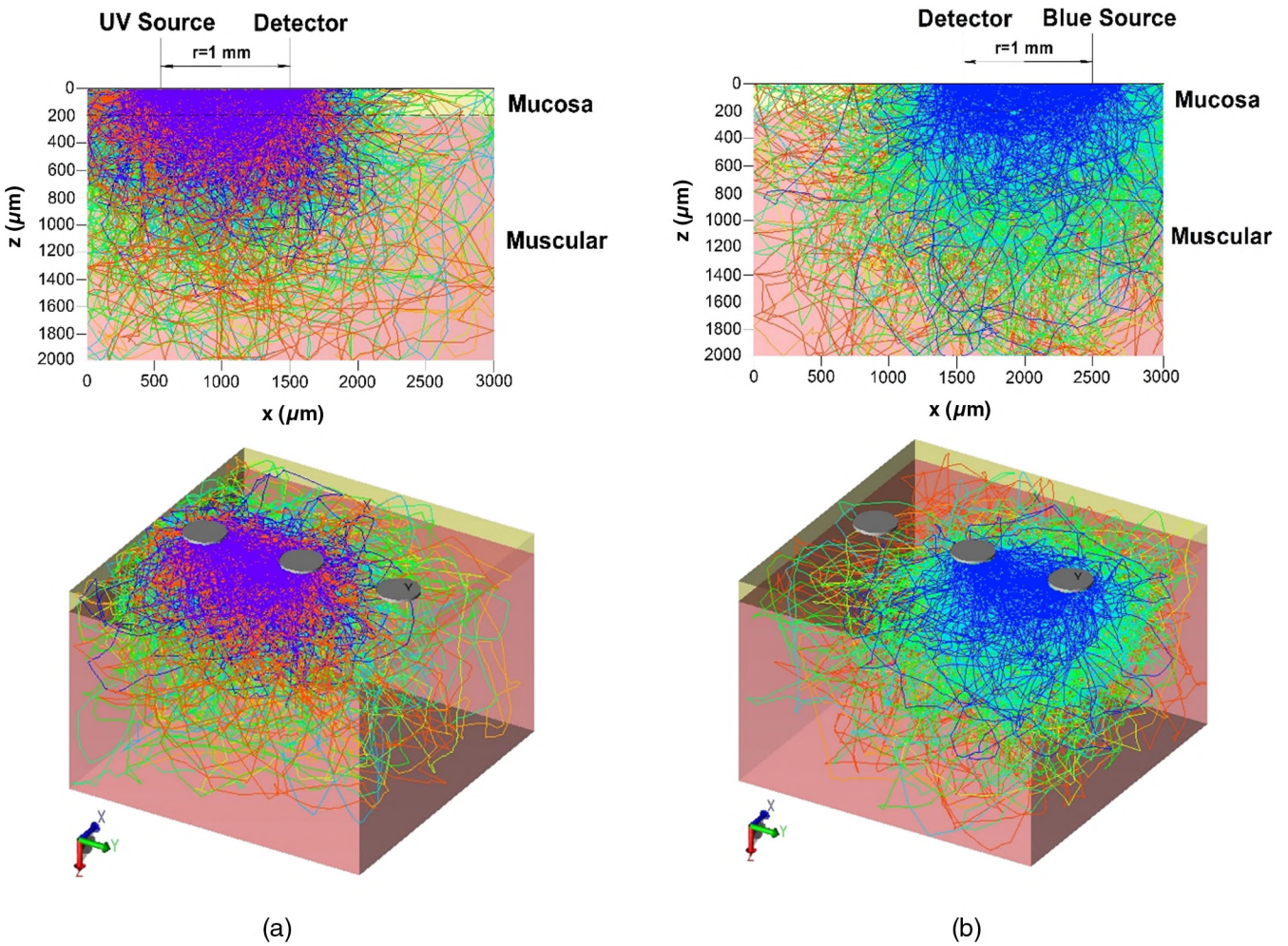

Fig. 4 (a) Side view and full 3-D view of model depicting simulated UV light within tissue. (b) Side view and full 3-D view of model depicting simulated blue light within tissue. For both sets, the source, detector, and the tissue layers are labeled. The lines indicate the passage of individual photons through the tissue.

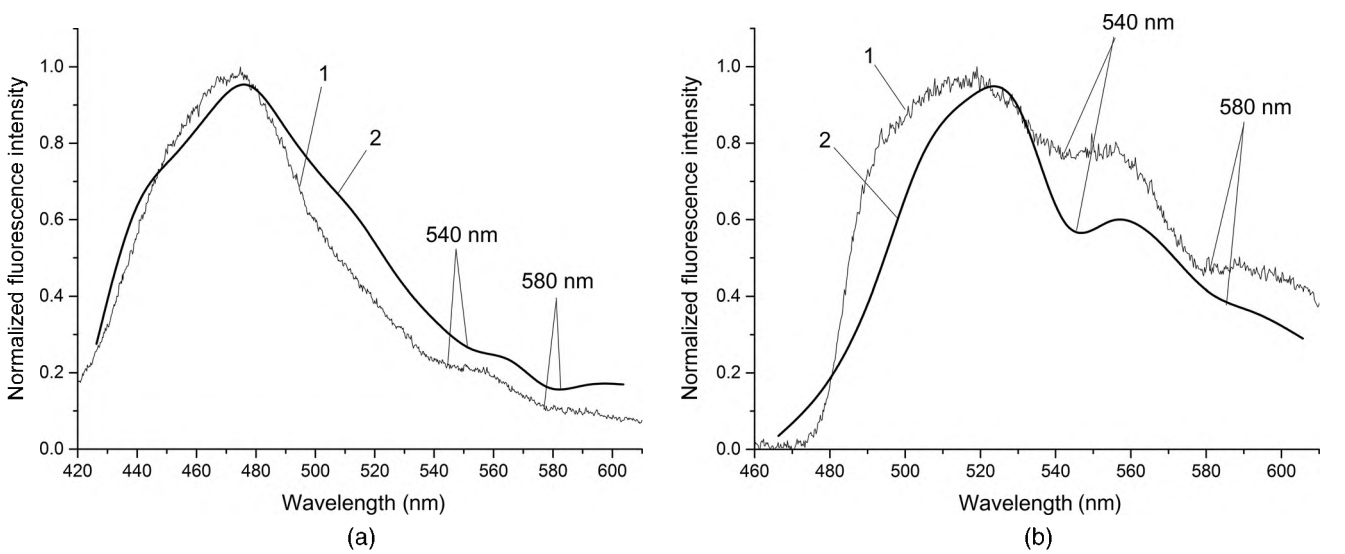

Fig. 5 Comparison of (1) experimental and (2) model-based spectra, calculated using the Monte-Carlo method. Model simulates presence of (a) NADH + collagen and (b) FAD + collagen.

ones. However, to date, the models have concentrated mainly on breast and cervix tissues, with none being produced or optimized for endoscopically reached hollow organs such as the bladder.

For the construction of our 3-D model, a two-layer setup was chosen. The physiological structure of the urinary bladder is easily simplified into two major layers, the muscle and the mucosa layers, without suffering in accuracy. This may be explained by the relatively large size of the modeled layers in comparison to omitted ones such as connective tissue. As the predominant constituent tissues of the bladder, they will be host to most of the tissue–light interactions. Other layers (e.g., connective tissue) would not drastically alter the model properties and would not be efficient to add to the model at this stage. Thus, these layers were not incorporated into the model. As the model described in this study was ultimately directed at aiding the detection of cancer, the contributing fluorophores selected were NADH, FAD, and collagen. These play a crucial role in observing tumor metabolism (through the redox ratio) and the structural extent of the tumor cells. Most of the other similar models, with the exception of Pavlova et al.[46] do not concentrate on FAD. The authors have found no similar models that look at the urinary bladder and incorporating the same fluorophores.

4.3 *Measured and Modeled Fluorescence*

Using the model, simulated fluorescence spectra can be produced. Upon comparison with experimentally measured tissue spectra, we can see a good consistency presented in Fig. 5. Some of the observable differences may be characterized by the presence of unaccounted for fluorophores within the real tissue. Additionally, other absorbing chromophores may contribute to the modification of the experimentally obtained spectrum. While these differences were also observable in the previously presented model,[36] this newer model displays marked advances. Figure 5 displays a higher level of accuracy to past work, where even the effects of blood (hemoglobin peaks at 540 and 580 nm) are clearly visible both on the experimental and modeled spectra. Furthermore, it is possible to conclude that the shape of the experimentally obtained bladder tissue fluorescence spectrum is heavily influenced by the fluorescence of present NADH and collagen (for 365 nm excitation) or FAD and collagen (for 450 nm excitation). A similar conclusion was reached by Drezek et al.[47] and Pavlova et al.[48] when studying cervical tissue using fluorescence microscopy. The studies reported that mitochondrial NADH and FAD dominate epithelial cell fluorescence.

4.4 *Future Prospects*

These very promising and substantial results demonstrate the ability of spectroscopic techniques to provide useful information for disease classification in a noninvasive manner. Although each of the techniques discussed in this article shows great potential as a means of detecting dysplasia in bladder, their combination should allow us to create a comprehensive picture of the biochemical and morphological stages of tissue. Specifically, fluorescence changes of biochemicals such as NADH, FAD and collagen will provide details about urinary bladder tissue biochemistry. This paper details marked improvements to our initial 3-D model by incorporating measured tissue data in favor of literature-based values. With further expansion of data sets and tissue types, this model has the potential to greatly aid in optical diagnostics of urinary bladder diseases such as cancer, when used in conjunction with other optical diagnostics tools. Combined with established methods of detection, use of such a model with non- or minimally invasive fluorescence measurements can aid in increasing the detection rate of BC, while helping reduce the number of false-positive diagnoses. Such improvements can lead to not only an increase in the quality of life of patients but also a great cost reduction and thus a reduction in the economical strain on health services. Use of human tissue can further improve the functionality of the model, advancing it in terms of accuracy and relevance. The use of both healthy and cancerous tissues can drastically improve the viability of this model in potential medical applications.

Additionally, based on the developed optical model and further computer simulations, the general distribution of light within tissue can be predicted. This can be invaluable in a variety of noninvasive optical methods of investigation.

5 Conclusion

Ultimately, the methods described in this paper can lead to potential new avenues of modeling and diagnostics. The model presented here can be refined to be more accurate and user friendly. This may result in a more effective clinical diagnostic tool capable of displaying a concise, but detailed visual data for end users. Furthermore, using similar techniques, the basic principles of the model can be expanded to diagnostics of other hollow organs and potentially even the heart.

Acknowledgments

This work was partially supported by the state task of the Ministry of Education and Science, Russian Federation, for the State University—Education-Science-Production Complex (basic part, No. 310). Special thanks are extended to Professor Lin Zhang for providing useful advice and help. Additional thanks to Dr. Victor V. Sidorov and Sergei Ravcheev of SPE "LAZMA," Moscow, Russia, and to Mohammed Al Araimi in the Lambda 1050 spectrophotometer core facility, School of Engineering and Applied Science, Aston University.

References

1. S. Xie, H. Li, and B. Li, "Recent progress in medical photonics," *Sci. China Ser. G* **52**(6), 856–863 (2009).
2. T. Vo-Dinh, Ed., *Biomedical Photonics Handbook*, CRC Press, Boca Raton (2010).
3. A. Jemal et al., "Cancer statistics, 2009," *CA. Cancer J. Clin.* **59**(4), 225–249 (2009).
4. K. D. Sievert et al., "Economic aspects of bladder cancer: what are the benefits and costs?" *World J. Urol.* **27**(3), 295–300 (2009).
5. I. Ahmad, O. J. Sansom, and H. Y. Leung, "Exploring molecular genetics of bladder cancer: lessons learned from mouse models," *Dis. Model. Mech.* **5**(3), 323–332 (2012).
6. A. van der Meijden, "Fortnightly review: bladder cancer," *Br. Med. J.* **317**(November), 1366–1369 (1998).
7. N. Ramanujam, "Fluorescence spectroscopy of neoplastic and non-neoplastic tissues," *Neoplasia* **2**(1–2), 89–117 (2000).
8. S. Palmer et al., "Technologic developments in the field of photonics for the detection of urinary bladder cancer," *Clin. Genitourin. Cancer* **11**(4), 390–396 (2013).
9. G. Mowatt et al., "Photodynamic diagnosis of bladder cancer compared with white light cystoscopy: systematic review and meta-analysis," *Int. J. Technol. Assess. Health Care* **27**(1), 3–10 (2011).

10. I. Karaoglu, A. G. van der Heijden, and J. A. Witjes, "The role of urine markers, white light cystoscopy and fluorescence cystoscopy in recurrence, progression and follow-up of non-muscle invasive bladder cancer," *World J. Urol.* **32**(3), 651–659 (2013).
11. R. O. P. Draga et al., "In vivo bladder cancer diagnosis by high-volume Raman spectroscopy," *Anal. Chem.* **82**(14), 5993–5999 (2010).
12. M. Anidjar et al., "Laser induced autofluorescence diagnosis of bladder tumors: dependence on the excitation wavelength," *J. Urol.* **156**(5), 1590–1596 (1996).
13. F. Koenig et al., "Laser induced autofluorescence diagnosis of bladder cancer," *J. Urol.* **156**(5), 1597–1601 (1996).
14. I. Georgakoudi, B. Jacobson, and M. Müller, "NAD (P) H and collagen as in vivo quantitative fluorescent biomarkers of epithelial precancerous changes," *Cancer Res.* **62**, 682–687 (2002).
15. V. Loschenov, V. Konov, and A. Prokhorov, "Photodynamic therapy and fluorescence diagnostics," *Laser Phys.* **10**(6), 1188–1207 (2000).
16. N. Akbar et al., "In vivo noninvasive measurement of skin autofluorescence biomarkers relate to cardiovascular disease in mice," *J. Microsc.* **255**(1), 42–48 (2014).
17. J. H. Ostrander et al., "Optical redox ratio differentiates breast cancer cell lines based on estrogen receptor status," *Cancer Res.* **70**(11), 4759–4766 (2010).
18. A. Walsh et al., "Optical imaging of metabolism in HER2 overexpressing breast cancer cells," *Biomed. Opt. Express* **3**(1), 75–85 (2012).
19. L. Brancaleon et al., "In vivo fluorescence spectroscopy of nonmelanoma skin cancer," *Photochem. Photobiol.* **73**(2), 178–183 (2001).
20. A. A. Stratonnikov et al., "Application of backward diffuse reflection spectroscopy for monitoring the state of tissues in photodynamic therapy," *Quantum Electron.* **36**(12), 1103 (2006).
21. D. Fielding et al., "Autofluorescence improves pretreatment mucosal assessment in head and neck cancer patients," *Otolaryngol.—Head Neck Surg.* **142**(3 suppl.), S20–S26 (2010).
22. M. C. Skala et al., "In vivo multiphoton microscopy of NADH and FAD redox states, fluorescence lifetimes, and cellular morphology in precancerous epithelia," *Proc. Natl. Acad. Sci. U. S. A.* **104**(49), 19494–19499 (2007).
23. A. Varone et al., "Endogenous two-photon fluorescence imaging elucidates metabolic changes related to enhanced glycolysis and glutamine consumption in precancerous epithelial tissues," *Cancer Res.* **74**(11), 3067–3075 (2014).
24. H. Aihara, H. Tajiri, and T. Suzuki, "Application of autofluorescence endoscopy for colorectal cancer screening: rationale and an update," *Gastroenterol. Res. Pract.* **2012**, 971383 (2012).
25. V. V. Tchernyi et al., "Some results of multiwave in situ autofluorescence diagnostics," *Proc. SPIE* **5693**, 336 (2005).
26. W. Zheng et al., "Optimal excitation-emission wavelengths for autofluorescence diagnosis of bladder tumors," *Int. J. Cancer* **104**(4), 477–481 (2003).
27. A. V. Dunaev et al., "Individual variability analysis of fluorescence parameters measured in skin with different levels of nutritive blood flow," *Med. Eng. Phys.* **37**(6), 574–583 (2015).
28. R. S. Bradley and M. S. Thorniley, "A review of attenuation correction techniques for tissue fluorescence," *J. R. Soc. Interface* **3**(6), 1–13 (2006).
29. H. Tajiri, "Autofluorescence endoscopy for the gastrointestinal tract," *Proc. Jpn. Acad. Ser. B. Phys. Biol. Sci.* **83**(8), 248–255 (2007).
30. K. Izuishi et al., "The Histological basis of detection of adenoma and cancer in the colon by autofluorescence endoscopic imaging," *Endoscopy* **31**(07), 511–516 (1999).
31. A. V. Bykov et al., "Multilayer tissue phantoms with embedded capillary system for OCT and DOCT imaging," *Proc. SPIE* **8091**, 80911R (2011).
32. M. S. Wröbel et al., "Multi-layered tissue head phantoms for noninvasive optical diagnostics," *J. Innov. Opt. Health Sci.* **8**(3), 1541005 (2015).
33. M. S. Wröbel et al., "Use of optical skin phantoms for preclinical evaluation of laser efficiency for skin lesion therapy," *J. Biomed. Opt.* **21**(8), 085003 (2015).
34. E. Okada and D. T. Delpy, "Near-infrared light propagation in an adult head model. II. Effect of superficial tissue thickness on the sensitivity of the near-infrared spectroscopy signal," *Appl. Opt.* **42**(16), 2915–2922 (2003).
35. K. L. Lurie et al., "Three-dimensional, distendable bladder phantom for optical coherence tomography and white light cystoscopy," *J. Biomed. Opt.* **19**(3), 36009 (2014).
36. I. Rafailov et al., "A novel excitation-emission wavelength model to facilitate the diagnosis of urinary bladder diseases," *Proc. SPIE* **9303**, 93030W (2015).
37. T. P. Moffitt, "Compact fiber-optic diffuse reflection probes for medical diagnostics," PhD Thesis, Western Washington University (2007).
38. S. A. Prahl, M. J. C. Van Gemert, and A. J. Welch, "Determining the optical properties of turbid media by using the adding–doubling method," *Appl. Opt.* **32**(4), 559–568 (1993).
39. V. V. Tuchin, *Tissue Optics: Light Scattering Methods and Instruments for Medical Diagnosis*, SPIE Tutorial Text in Optical Engineering, SPIE Press, Washington (2000).
40. H. van Staveren, "Integrating sphere effect in whole bladder wall photodynamic therapy at violet, green, and red wavelengths," *Proc. SPIE* **2323**, 13–20 (1995).
41. OriginLab, "Curve fitting functions," in *Manual*, pp. 1–166 (2000).
42. I. Pavlova et al., "Understanding the biological basis of autofluorescence imaging for oral cancer detection: high-resolution fluorescence microscopy in viable tissue," *Clin. Cancer Res.* **14**(8), 2396–2404 (2008).
43. R. Drezek et al., "Understanding the contributions of NADH and collagen to cervical tissue fluorescence spectra: modeling, measurements, and implications," *J. Biomed. Opt.* **6**(4), 385–396 (2001).
44. G. Palmer and N. Ramanujam, "Monte-Carlo-based model for the extraction of intrinsic fluorescence from turbid media," *J. Biomed. Opt.* **13**(2), 024017 (2008).
45. C. Zhu et al., "Model based and empirical spectral analysis for the diagnosis of breast cancer," *Opt. Express* **16**(19), 14961–14978 (2008).
46. I. Pavlova et al., "Fluorescence spectroscopy of oral tissue: Monte Carlo modeling with site-specific tissue properties," *J. Biomed. Opt.* **14**(1), 014009 (2009).
47. R. Drezek et al., "Autofluorescence microscopy of fresh cervical-tissue sections reveals alterations in tissue biochemistry with dysplasia," *Photochem. Photobiol.* **73**(6), 636 (2001).
48. I. Pavlova et al., "Microanatomical and biochemical origins of normal and precancerous cervical autofluorescence using laser-scanning fluorescence confocal microscopy," *Photochem. Photobiol.* **77**(5), 550 (2003).

Biographies for the authors are not available.